Electrochemical characteristics of sugarcane bagasse-activated carbon as cathode material of lithium-ion capacitors

Murie Dwiyaniti[a] • Luh Krisnawati[a] • Agus Edy Pramono[b] •
Achmad Subhan[c] • Rudy Setiabudy[a] • Chairul Hudaya[a,d]*

[a]Department of Electrical Engineering, Faculty of Engineering, Universitas Indonesia,
[b]Departement of Mechanical Engineering, Politeknik Negeri Jakarta, Jl Prof Dr GA Siwabessy, Indonesia
[c]Research Center for Advanced Materials-National Research and Innovation Agency (BRIN)
[d]Research Center for Energy and Environment, Sumbawa University Technology, West Nusa Tenggara, Indonesia

Abstract: Investigation of the physical and electrochemical characterization of the sugarcane bagasse-derived activated carbon (SBAC) as a cathode material of lithium-ion capacitor (LIC) was reported in this article. The as-prepared SBAC was tested by BET, SEM, and EDS characterization. SBAC was assembled as cathode material and lithium titanate oxide (LTO) as anode material used to fabricate LIC in a CR2032 coin cell. The results show the as-synthesized SBAC has a microporous architecture with a surface area of 1,906 m^2/g. The developed LIC exhibited an energy density of 28.4 Wh/kg and a power density of 1,770 W/kg, and a capacity retention of 75% at 100 cycles. In addition, this LIC has a specific capacitance of 141.8 mF/g. This study indicates that sugarcane bagasse is a prospective carbonaceous material for the cathode of LIC.

*Corresponding author.
E-mail address: c.hudaya@eng.ui.ac.id (Chairul Hudaya).

1. Introduction

The utilization of renewable energy requires energy storage, supplied mainly by batteries, due to the intermittent nature (Das et al., 2019; Zeng et al., 2019). The latest energy storage technologies widely used for this purpose are lithium-ion batteries (LIB) and supercapacitors. LIB provides relatively large energy density, long cycle life, and minimal maintenance. However, it takes a long to charge and discharge (Nitta et al., 2015). In contrast, the supercapacitor has a high power density of about 10 kW/kg, so the charging and discharging process can be done rapidly in milliseconds order (Da Silva et al., 2020; Xie et al., 2018). Unfortunately, its energy density is only about 5.10 Wh/kg, so it cannot store a large amount of energy (Conway, 2013; Simon & Gogotsi, 2010).

It is desirable that energy storage technologies should provide both high energy and power densities. A technology integrating the features of battery and supercapacitor is created to achieve this goal, namely a hybrid supercapacitor or a lithium-ion capacitor (LIC) (Ju et al., 2019; Lin et al., 2021). It consists of a supercapacitor's electrode as the positive electrode (cathode) to produce high power and a lithium-based electrode as the negative electrode (anode) to yield a high energy density.

LIC research has resulted in an energy density of ~ 10-100 Wh/kg and a power density of ~ 1-10 kW/kg (Jagadale et al., 2019). The value of energy and power density is strongly influenced by the design and material characteristics of the anode, cathode, and electrolyte. In this study, the anode material used is LTO ($Li_4Ti_5O_{12}$). The cathode material used is activated carbon. The focus of this research is the cathode material made of activated carbon.

The ideal requirement for activated carbon to be used as cathode material of LIC is to have a large pore volume, a microporous pore diameter of 0.8-1.4 nm, and a large surface area > 3,000 m^2/g (Li et al., 2016). Graphene was proposed because it provides a high surface area of 3,355 m^2/g and 147 Wh/kg (Zhang et al., 2013).

However, graphene is still expensive, has a complicated manufacturing process, and has hazardous fabrications (Zurutuza & Marinelli, 2014). Thus, researchers are looking for other activated carbon materials that are low-cost, easy to manufacture, non-toxic, and environmentally friendly. One of the activated carbon materials that are estimated to be able to meet these requirements is sugarcane bagasse biomass waste. This waste is abundant; during the sugar manufacturing process, only 8% of sugar cane is used for sugar, while 30% of it becomes waste in the form of bagasse (Tajalli, 2015).

Sugarcane bagasse is a lignocellulosic material that has the potential to become good-quality activated carbon. In the process of synthesizing biomass waste into activated carbon, most of the studies use the hydrothermal method (Azad et al., 2016; S. Liu et al., 2010) and pyrolysis through inert nitrogen gas in the reactor (Adinaveen et al., 2013) or argon (Rahma et al., 2019; Dwiyaniti et al., 2020). However, few researchers utilize the pyrolysis method with airtight reactor tubes without flowing inert gas (nitrogen or argon) (Pramono et al., 2019). In fact, by using this method, the synthesis process saves production time and cost because it does not require an inert gas, and the as-prepared product does not require any washing prior to carbonization. In addition, most researchers use the wet method in which the activated carbon is mixed with an activating agent in the solution. Thus, this process takes a long time because it needs to be stirred and dried leading to an elevated cost.

In this study, synthesizing sugarcane bagasse into activated carbon was simplified. The pyrolysis method used an airtight reactor tube, and activation was carried out using the dry method. In the dry means, the chemical activator is mixed directly into the carbon without a solution. This study aims to investigate the physical characteristics of sugarcane bagasse activated carbon and the electrochemical characteristics of LIC made of sugarcane bagasse activated carbon.

2. Materials and methods

Sugarcane bagasse comes from the sugar factory PT Gendhis Multi Manis, Indonesia. The experimental works in this study consisted of five stages: preparation of raw materials, carbonization, activation process, LIC assembly, and characterizations. In making activated carbon, we followed steps from other studies (Dwiyaniti et al., 2020; Rahma et al., 2019). The difference is the cooking process which uses an airtight reactor tube.

2.1. Preparation of raw materials

Sugarcane bagasse from the sugar factory was dried in an oven at 80 °C for 24 hours to remove moisture. The samples were blended for 10 minutes and then sieved through a 100-mesh sieve. This process produces dry bagasse powder with an estimated size of 149 microns.

2.2. Carbonization

The sugarcane bagasse powder was carbonized by the pyrolysis method. The Furnace equipment used an airtight reactor tube at a temperature of 500 °C, with a heating rate of 2 °C/min. The temperature was maintained for 2 hours. The result of this stage was called the sugarcane bagasse carbon (SBC).

2.3. Activated carbon

Activated carbon is used to increase the pore volume and specific surface area. The activating agent used in this study was KOH. KOH in the form of crystals was crushed and then

mixed with carbon. In this process, mixing did not use a solution, so the process became more straightforward and faster. The mass ratio of carbon and KOH used in this study was 1:2, 1:3, and 1:4. After mixing, the process was continued by cooking carbon + KOH in an airtight reactor tube furnace at a temperature of 800 ^{O}C with a heating rate of 2 ^{O}C/min and maintained for 2 hours. The activation results were naturally cooled and then washed by dissolving it in HCl to obtain a neutral pH, followed by washing it with distilled water. Furthermore, these samples were called sugarcane bagasse-activated carbon SBAC12, SBAC13, and SBAC14.

2.4. Fabrication of LIC

The fabrication of LIC consists of three stages: the fabrication of cathode, anodes, and assembly of LIC in a CR2032 coin cell arrangement.

2.4.1. Cathode fabrication

The cathode fabrication procedure has four stages: slurry making, casting, drying, and printing. The process began with sieving the SBAC using 400 mesh to produce a powder of 37 microns. The ingredients for the slurry were SBAC, polyvinylidene fluoride (PVDF), and super-P (acetylene black) with a mass ratio of 85:10:5. The first process in the slurry making was mixing PVDF with NMP solution and stirring the material with a magnetic stirrer at a rotational speed of 800 rpm with a temperature of 80 ^{O}C for 15 minutes. The second process was mixing the super-P and SBAC using a pestle mortar until smooth. Then this material was divided into three parts and gradually added to the PVDF and NMP solutions at an interval of 10 minutes. After then, all slurry was stirred until it was homogeneous. The following process was casting by pouring the slurry material on an aluminum foil sheet using a doctor blade coating machine. Casting was carried out with thickness parameters of 200 μm. The process of flattening the cathode sheet used a rolling press to produce homogeneity on each side. Then it dried again at a temperature of 80 ^{O}C for 10 minutes.

2.4.2. Anode fabrication

The manufacturing process of the anode was the same as that of the cathode. However, the slurry material and the casting sheet were the only difference. The mass ratio of slurry materials for the anode was 80:10:10 for the LTO, PVDF, and Super-P, respectively. The slurry was poured on top of a battery-grade copper foil sheet during the casting process.

2.4.3. LIC assembly

After the electrode manufacturing process was complete, the cathode and anode sheets were printed in a circle using a coin cell cutter with a size according to the diameter of the CR2032 coin cell. The LIC arrangement was carried out from the base to the cover, namely the cell base, cathode, separator, anode, spacer, spring, and cell cover.

2.5. Materials and cells characterization

The material characterization used five tests, namely (1) XRD (X-Ray Diffraction) using the Panalytical X'PERT-3 Powder with step size 0.0260, Cu K-Alpha radiation (k=1.54060 A); (2) FTIR using Shimadzu IR Prestige 21; (3) Brunauer-Emmet-Teller (BET) using the QuantachromeNovaWin instrument, with nitrogen degassing for 4 hours to determine the surface area of activated carbon; (4) scanning electron microscopy (SEM) using Zeiss EVO10 to determine the shape and surface structure of the sample visually; (5) energy dispersive spectroscopy (EDS) using Zeiss EVO10 to determine chemical elements in SBAC. Meanwhile, the electrochemical test consists of three tests, namely (1) cyclic voltammetry (CV), (2) charge-discharge (CD) using WBCS3000, and (3) electrochemical impedance spectroscopy (EIS) using Hioki 3522-50.

3. Results and discussion

3.1. Synthesis of sugarcane bagasse into activated carbon

Carbonization by pyrolysis method aimed to produce amorphous carbon, high oxygen content, and porous structure. The composition of sugarcane bagasse, which consisted of hemicellulose, cellulose, and lignin, would degrade at a specific temperature during cooking. Dehydration and decomposition of hemicellulose released CO and CO_2 gases at a temperature of 220–315 ^{O}C, cellulose at 315–400 ^{O}C, and lignin at 160-900 ^{O}C (Yang et al., 2007). This process caused a reduction in volatile matters resulting in mass shrinkage. The higher the cooking temperature, the more the carbon mass shrinks. This phenomenon also happened in this study. The cooking process at a temperature of 500 ^{O}C using the airtight reactor tube pyrolysis method produced a mass shrinkage of 40%, while the rest was the yield. However, this result was still higher when compared to other studies that used pyrolysis with an inert gas stream (argon or nitrogen). The average mass shrinkage in the pyrolysis method with the inert gas flow is 75-85%, meaning resulting yields of 15-25% (Hidayati et al., 2016; Oliveira et al., 2013; Pandey et al., 2000). The increasing shrinkage in the pyrolysis of the inert gas is probably caused by the inert gas flow binding the impurities and carrying them out from the furnace. It is proved by the changing colour of filter water in which the watercolour becomes darker.

3.2. Analysis of the crystallographic and functional structure

The XRD pattern, as shown in Figure 1, showing carbon structure, which tends to be amorphous, is indicated by broad and weak diffraction peaks.
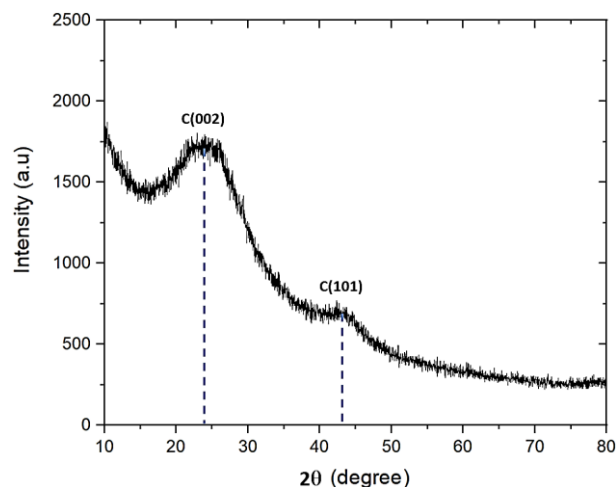
Figure 1. XRD patterns for sugarcane bagasse activated carbon.

The XRD pattern of sugarcane bagasse carbon exhibits two board diffraction peaks. The board diffraction peak at 2θ angles of 24.36^O and 43.8^O was identified as the graphite (002) and (101) structures, respectively (X. Liu et al., 2010; Lu et al., 2017; Okamura et al., 2006). The broad (002) band indicates a low crystallinity, which comprises both amorphous carbon and aliphatic side chains (Rajarao et al., 2014).

Figure 2 shows the FTIR spectra to clarify the functional groups on the sugarcane bagasse surface before and after activation. Examining the functional groups of sugarcane bagasse carbon follows that in reference (Kumar et al., 2019).

The area peaks between 1400–1650 cm−1 and 3200–3700 cm−1 show the C=C stretching bond of the aromatic ring and the O-H (hydroxyl) groups, respectively, which are significantly weaker after activation. The decrease in C=C stretching vibration intensity is due to the oxygenation of the graphitic carbon matrix. The self-cracking of chars damaged the O-H groups and released H_2 and CO (Lu et al., 2017).

The peak area between 1000 - 1300 cm^{-1} is the vibration mode of C-O. The intensity of C-O groups increased after activation. In addition, after the activation process, a new absorption is formed at 2065 cm^{-1} of C≡C triple carbon bond and wave number 800 cm^{-1} of an aromatic C-H.

The presence of O-H and C-O bonds indicates that the activated carbon from the sugarcane bagasse tends to be more polar. However, there are still C=C and C≡C bonds which are non-polar (Wibowo et al., 2011).
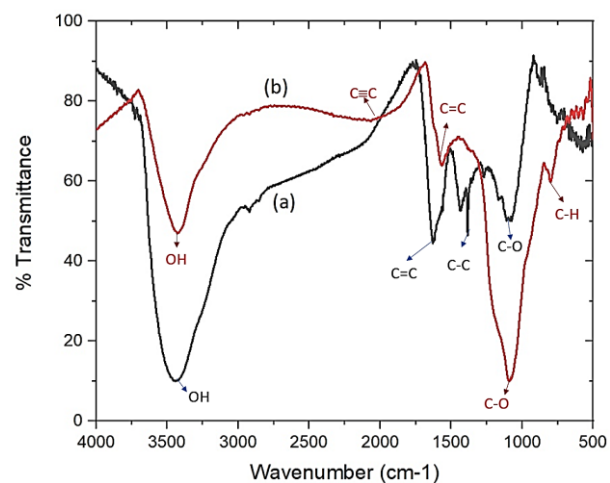
Figure 2 FTIR spectra of sugarcane bagasse carbon (a) before and (b) after activated.

3.3. Analysis of surface morphological

Scanning electron microscopy (SEM) test was conducted to reveal the surface morphology of activated carbon. Before carrying out the test, the activated carbon sample was coated with gold to make the sample more conductive. SEM testing was carried out at 1000x, 5000x, and 10000x magnification. The results of the SEM test can be seen in Figure 3.

Most of the surface morphologies of SBAC have a hexagonal hollow pore structure with varying pore depth and length. This surface morphology is typical to those found in various activated carbons made from biomass with chemical activation (Das et al., 2015; Rahma et al., 2019; Salman, 2014;Timur et al., 2006).
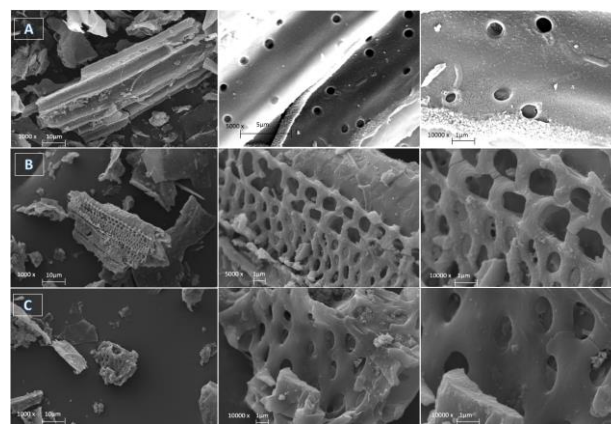
Figure 3. SEM test results on (A) SBAC12, (B) SBAC13, (C) SBAC14.

SEM images were also analyzed using OriginLab software to predict surface porosity. The porosity was determined by calculating the volume beneath the surface and the volume

beneath a flat surface, the height of which is equal to the maximum height of any point on the sample's surface (Abdullah & Khairurrijal, 2009).
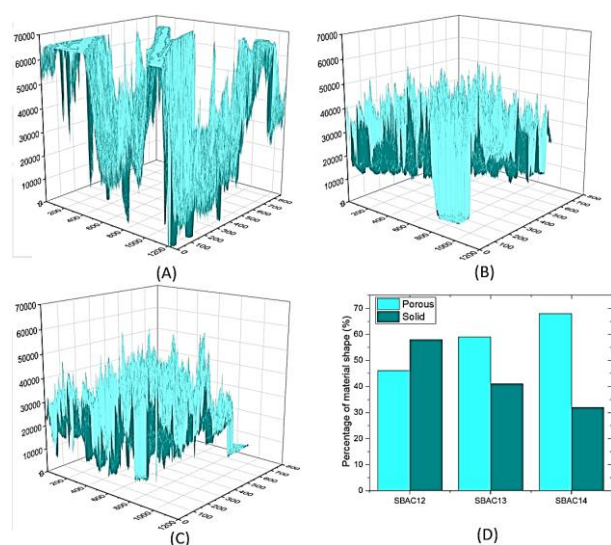
Figure 4. The comparison of porous and solid material on the surface of (A) SBAC12, (B) SBAC13, and (C) SBAC14.

Quantitatively, Figure 4 compares the pores distribution of SBAC surfaces. The SBAC14 had the highest surface porosity at 68%, followed by SBAC13 at 59% and SBAC12 at 46%. The surface porosity in SBAC12 appears to have a wide range of size variations and a less dense surface porosity, as shown in Figure 4A. Meanwhile, the surface porosity in SBAC13 and SBAC14 appears to have a smaller size variations range, tending to be the same, with a denser surface porosity, as shown in Figure 4B and 4C. The difference in surface porosity in the surface morphology occurred due to the addition of the KOH activator agent to carbon.

3.4. Analysis of elemental composition

Activated carbon originated from natural materials/ biomass mostly contains carbon compounds and minerals. Some of these minerals would be removed during the carbonization and activation process. The elemental composition of activated carbon was determined using energy dispersive spectroscopy (EDS), as shown in Figure 5. In this case, the elemental composition of SBAC12 was observed.

Chemical reactions that occur upon activation (Nowrouzi et al., 2017):

$4KOH(aq)+C(s){\rightarrow}K_2CO_3(aq)+K_2O(aq)+2H_2(g)$ (1)
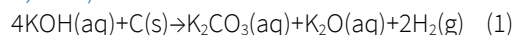
Based on Equation (1), the chemically activated SBAC product contains K, C, O, and H elements. The sample should be washed with acidic HCl and distilled water to remove undesired elements, such as K. Then, it was dried in the oven and characterized using EDS.
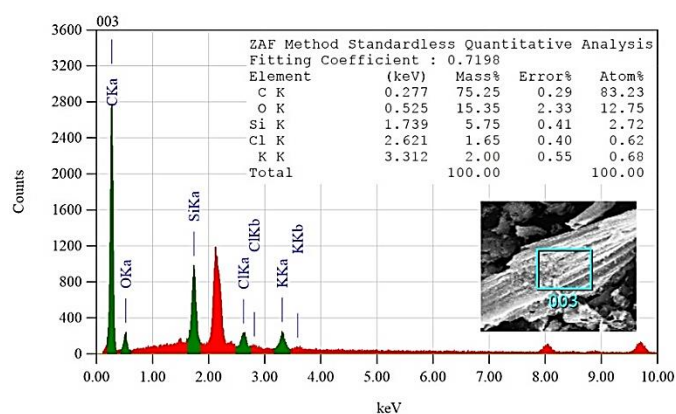
Figure 5. Elemental composition of SBAC12.

As shown in Figure 5, SBAC has the dominant element C (carbon) with a percentage of more than 80% and some others O, Si, Cl, and K, which indicates that the method used in this study has succeeded in synthesizing bagasse into activated carbon. The same results were obtained by most of the researchers who used the pyrolysis method with an inert gas (Barruna et al., 2021; Dwiyaniti et al., 2020; Guo et al., 2020; Luo et al., 2019). The dominant carbon content would affect the ion adsorption process in LIC.

In the EDS results, there was also an element of Si, which was the main content of sugarcane bagasse left behind during the activation process. In contrast, K elements were residues from activation with KOH with less contents (< 5%). Meanwhile, the Cl element was a residue from washing activated carbon. The presence of the small amount of K and Cl elements indicated that the activated carbon washing process was successfully conducted.

3.5. Analysis of specific surface area

The Brunauer-Emmet-Teller (BET) test was carried out to measure the pore diameter, pore volume, and specific surface area (SSA) of SBAC. One parameter that affects the SSA of carbon is the use of KOH. Adding KOH can accelerate the reaction of pore formation; however, when excessive KOH is added, pore structure damage occurs. Table 1 shows the SSA, total pore volume, micropore volume and average pore diameter of SBAC. The SBAC14 exhibits the highest SSA of about 1,906 m^2/g. This value is relatively higher compared to similar precursors (El Naga et al., 2019; Guo et al., 2020; Jain & Tripathi, 2015).

Table 1. The BET test results of SBAC12, SBAC13, and SBAC14.

Sample	$^aS_{BET}$ (m^2/g)	^bV_t (cm^3/g)	^cV_m (cm^3/g)	^dD_p (nm)
SBAC12	866	0.77	0.35	2.18
SBAC13	992	0.94	0.56	1.74
SBAC14	1906	1.49	0.76	1.65

$^aS_{BET}$: *specific surface area calculated by the BET method*
^bV_t: *total pore volume calculated at P/P0= 0.99*
^cV_m: *micropore volume calculated by the t-plot method*
^dD_p: *average pore diameter*

According to IUPAC (International Union of Pure and Applied Chemistry), based on the pore diameter or porosity, activated carbon can be divided into three, namely macropores having a pore diameter of >50 nm, mesopores having a pore diameter of 2 nm – 50 nm, and micropores having a pore diameter of <2 nm. The BET test results in Table 1 show that SBAC12 had an average pore diameter of 2.18 nm (mesopore). Meanwhile, SBAC13 and SBAC14 had an average pore diameter of <2nm (micropores).

3.6. Analysis of cyclic voltammetry (CV)

In the CV test, SBAC (cathode) and LTO (anode) were assembled in coin cell CR2032, and it is known that this sample was referred to as SBAC12/LTO, SBAC13/LTO, and SBAC14/LTO cells. CV is a method of measuring electrochemical properties that displays the relationship between current and voltage. CV testing produces a hysteresis-shaped curve, where the wider the curve, the greater the capacitance value. In this study, the CV test was carried out in a voltage range of 1-3 V in the scan rate of 5, 10, and 15 mV/s. The scan rate variation aims to determine how fast the potential rate of electrons is marked by an increase in the current (Savéant, 2006). The CV test result curve is shown in Figure 6.

As LIC is a combination of LIB and supercapacitor, the resulting CV curve usually shows the combination of both reactions. The CV curves of LIB generally have peaks representing a pair of redox reactions occurring at the electrode surface. In comparison, the ideal supercapacitor CV curve is almost rectangular form. The results of the CV test in this study (Figure 6) showed that the SBAC12/LTO, SBAC13/LTO, and SBAC14/LTO cells had a curved shape resembling a leaf shape known as a quasi-square shape. However, the CV results did not appear to have peaks which are characteristic of the redox reaction at LIC as in the reference (Chen et al., 2021; He et al., 2018; Lin et al., 2021). This is expected because the FTIR results (Figure 2) on the cathode material derived from sugarcane bagasse active carbon did not have a carboxyl (C=O) functional group. The carbonyl

functional group is essential in the process of electron transfer (redox reaction) (Chen et al., 2021; He et al., 2018).

When the voltage was less than 1.5 V, the SBAC/LTO cell showed no apparent electrochemical activity. Since the SBAC/LTO could store charge through the insertion of Li+ ions only at voltages greater than 1.5 V, the redox reactions limit the potential for Li+ insertion in SBAC /LTO (Lin et al., 2021).

When the scan rate was increased from 5 – 15 mV/s, it was found that the increasing values lead to an increase in current. Figures 6A, B, and C show that all cells had high currents at a scan rate of 15 mV/s; this happened because the applied voltage provided enough energy to the electrons to travel faster in the system.
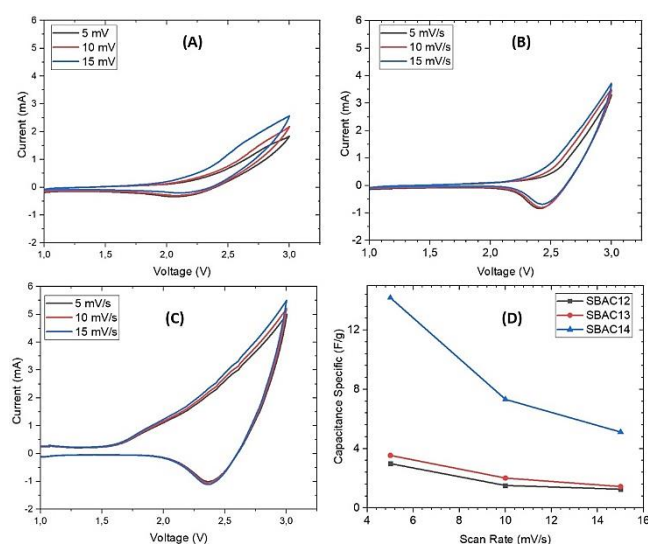
Figure 6. CV test curve at 1-3V voltage and scan rate 5, 10, and 15 mV/s at (A) SBAC12/LTO, (b) SBAC13/LTO, (C) SBAC14/LTO, and (D) specific value of capacitance.

Furthermore, the scan rate also affected the curve area, which impacted the cell-specific capacitance value. The specific value of capacitance can be calculated using Equation (2).

$$C_p = \frac{A}{2mk(\Delta V)} \quad (2)$$

Where C_p is the specific capacitance (F/g), A is the area inside the CV curve (m^2), m is the mass of the material (g), k is the scan rate (V/s), and (V_2-V_1) is the window voltage (V).

Based on Figure 6D, the smallest CV area was obtained by sample SBAC12, while the largest area was obtained by sample SBAC14. The specific capacitance value got smaller as the scan rate got higher. This was in accordance with the rules of Equation 2, where the specific capacitance value was inversely proportional to the scan rate. The largest specific capacitance value was 14.18 F/g produced by SBAC14 at a scan rate of 5 mV/s. Meanwhile, the specific capacitance for SBAC13/LTO and SBAC12/LTO was 3.55 F/g and 2.99 F/g, respectively.

The formula to determine the specific power (P) and specific energy (E) of SBAC/LTO using Equations (3) and (4).

$$E = \frac{1}{2} C_p (\Delta V)^2 \qquad (3)$$

$$P = \frac{E}{t} \qquad (4)$$

Where E is specific energy (Wh/kg), C_p is specific capacitance (F/gr), ΔV is potential window (V), P is specific power (W/kg), and t is discharging time (sec).

Maximum specific energy of 5.9 Wh/kg, 7.1 Wh/kg, and 28.4 Wh/kg was obtained for SBAC12/LTO, SBAC13/LTO, and SBAC14/LTO, with the maximum power density of 1,420 W/kg, 1,680 W/kg, and 1,770 W/kg respectively.

3.7. Analysis of charge discharge (CD)

CD testing determines the performance and life cycle of energy storage cells. In this study, the CD test was carried out in a voltage range of 1-3 V with constant current variations of 250, 375, and 500 µA/g. The results of the CD test are shown in Figure 7.

Based on Figure 7, the larger the current, the faster the charging and discharging process. Ideally, the discharge time should equal or be less than the charge time. However, in our test data, the discharge time was faster than the charging time. An unwanted irreversible reaction was suspected to occur at the electrodes, causing rapid degradation of the electrodes. Electrode degradation caused an increase in internal resistance resulting in a voltage drop. This phenomenon is similar to the characteristics of CD sugarcane bagasse for supercapacitor applications in ref (Jain & Tripathi, 2015). There was a sudden drop in the potential due to ohmic resistance associated with the device. This test also strengthened the calculation of the power density in the CV test, in which the resulting power density was related to the charge and discharge current density.

The charge-discharge cycle performance was also conducted at a scan rate of 250 µA/g and the results were shown in Figure 7D. After 100 cycles, there was a significant drop in SBAC12/LTO and SBAC13/LTO. However, the SBAC14/LTO tended to be stable, and the capacity retention percentage was 75% at the end cycle.

3.8. Analysis of electrochemical impedance spectroscopy (EIS)

One of the most critical parameters of a battery system is conductivity. The Four Point Probe method can measure a single cathode sheets conductivity. However, considering these sheets are arranged together with other battery compo-

nent sheets, the conductivity measurement was carried out through AC Impedance using an electrochemical impedance spectroscopy (EIS) tool. The measurement of conductivity in the Nyquist graph is shown in Figure 8. The conductivity was calculated using Equation (5) based on the figure.

$$\sigma = \frac{t}{A\,R_{sum}} \qquad (5)$$

Where t is the sample thickness (cm), A is the sample surface area (cm^2), R_{sum} is the total impedance of the reel (Ω), and σ is the ionic conductivity (S/cm).
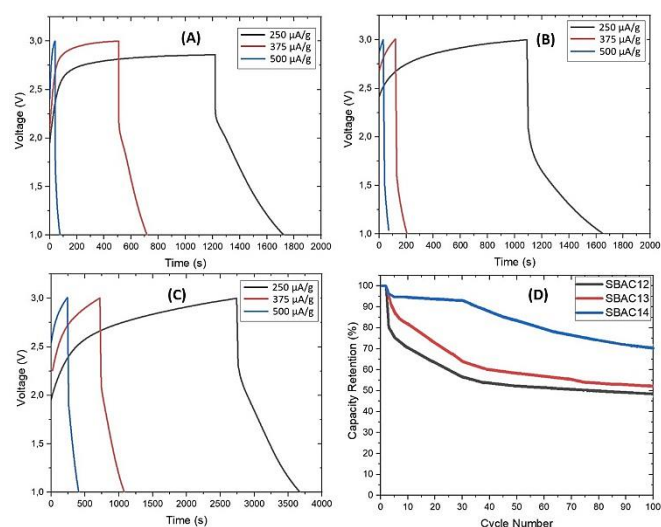
Figure 7. CD test curve at a 1-3V voltage and scan rates of 250, 375, and 500 µA/s at (A) SBAC12/LTO, (B) SBAC13/LTO, (C) SBAC14/LTO, and (D) the percentage of capacity retention at a scan rate of 250 µA/s for 100 cycles.

The desired conductivity of a LIC was large because the conductivity value significantly affects the electron travel and the lithium-ion diffusion distance.

The greater the conductivity, the shorter the electron travel and lithium-ion diffusion distance; this will speed up the process of charging electrons from the anode to the cathode. Based on the formula in Equation 5, the conductivity value of SBAC12/LTO was 1.14 µS/cm, SBAC13/LTO was 2.21 µS/cm, and SBAC14/LTO was 6.59 µS/cm. The straight line in the Nyquist image showed the diffusion process of lithium ions into the electrode material, where the excellent intercalation process was at an angle of 45^0 (Sun et al., 2018). Based on Figure 8, SBAC14/LTO had a slope angle close to 45^0, indicating that the lithium-ion intercalation process in the electrode material has been running well.
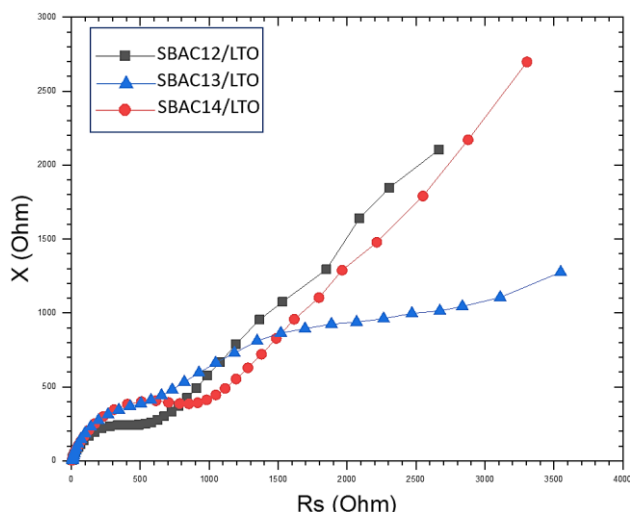
Figure 8. Nyquist plot on SBAC12/LTO, SBAC13/LTO, and SBAC14/LTO conductivity.

4. Conclusion

The physical and electrochemical characteristics conducted in this study reveal the feasibility of the activated carbon derived from sugarcane bagasse for the cathode material of LIC. The optimum sample is the mass ratio of carbon to KOH that reaches 1:4, which has a maximum surface area of 1,906 m^2/g. The electrochemical characterization of SBAC14/LTO delivers an energy density of 28.4 Wh/kg, a power density of 1,770 W/kg, capacity retention of 75% at 100 cycles, a capacitance of 141.8 mF/g, and high conductivity of 6.59 µS/cm. This study suggests that sugarcane bagasse-derived activated carbon could be a promising electrode for cost-effective manufacture of high-energy and power of electrochemical energy storage devices. Also, it certainly helps us keep the environment safe by recycling biowaste into a useful one.

Conflict of interest

The authors have no conflict of interest to declare.

Acknowledgments

Funding

References

Abdullah, M., & Khairurrijal, K. (2009). A Simple Method for Determining Surface Porosity Based on SEM Images Using OriginPro Software. *Indonesian Journal of Physics*, *20*(2), 37-40. https://doi.org/10.5614/itb.ijp.2009.20.2.4

Adinaveen, T., Kennedy, L. J., Vijaya, J. J., & Sekaran, G. (2013). Studies on structural, morphological, electrical and electrochemical properties of activated carbon prepared from sugarcane bagasse. *Journal of Industrial and Engineering Chemistry*, *19*(5), 1470–1476. https://doi.org/10.1016/j.jiec.2013.01.010

Azad, F. N., Ghaedi, M., Dashtian, K., Hajati, S., & Pezeshkpour, V. (2016). Ultrasonically assisted hydrothermal synthesis of activated carbon–HKUST-1-MOF hybrid for efficient simultaneous ultrasound-assisted removal of ternary organic dyes and antibacterial investigation: Taguchi optimization. *Ultrasonics sonochemistry*, *31*, 383-393. https://doi.org/10.1016/j.ultsonch.2016.01.024

Barruna, A. E., Naufal, R. M., Nugraha, M. R., Subiyanto, I., Tinaprilla, N., Subhan, A., & Chairul, H. (2021). Material characteristics and electrochemical performance of lithium-ion capacitor with activated carbon cathode derived from sugarcane bagasse. In IOP Conference Series: Earth and Environmental Science (Vol. 673, No. 1, p. 012018). IOP Publishing.

Chen, J., Li, C., Lian, Y., Chen, Y., Chen, T., & Hu, X. (2021). Understanding the oxygen-containing functional groups on multiwall carbon nanotubes toward supercapacitors. *Materials Today Chemistry*, *19*, 100414. https://doi.org/10.1016/j.mtchem.2020.100414

Conway, B. E. (2013). Electrochemical supercapacitors: scientific fundamentals and technological applications. Springer Science & Business Media. https://doi.org/10.1007/978-1-4757-3058-6

Da Silva, L. M., Cesar, R., Moreira, C. M., Santos, J. H., De Souza, L. G., Pires, B. M., ... & Zanin, H. (2020). Reviewing the fundamentals of supercapacitors and the difficulties involving the analysis of the electrochemical findings obtained for porous electrode materials. *Energy storage materials*, *27*, 555-590. https://doi.org/10.1016/j.ensm.2019.12.015

Das, D., Samal, D. P., & Meikap, B. C. (2015). Preparation of activated carbon from green coconut shell and its characterization. *J. Chem. Eng. Process Technol*, *6*(5), 1-7. https://doi.org/10.4172/2157-7048.1000248

Das, P., Wu, Z.-S., Li, F., Liang, J., & Cheng, H.-M. (2019). *Two-dimensional energy materials: opportunities and perspectives*. Elsevier. https://doi.org/DOI:10.1016/j.ensm.2019.03.014

Dwiyaniti, M., Barruna, A. G. E., Naufal, R. M., Subiyanto, I., Setiabudy, R., & Hudaya, C. (2020). Extremely high surface area of activated carbon originated from sugarcane bagasse. *IOP Conference Series: Materials Science and Engineering*, *909*(1), 12018. https://doi.org/doi:10.1088/1757-899X/909/1/012018

El Naga, A. O. A., El Saied, M., Shaban, S. A., & El Kady, F. Y. (2019). Fast removal of diclofenac sodium from aqueous solution using sugar cane bagasse-derived activated carbon. *Journal of Molecular Liquids*, *285*, 9-19. https://doi.org/10.1016/j.molliq.2019.04.062

Guo, Y., Tan, C., Sun, J., Li, W., Zhang, J., & Zhao, C. (2020). Porous activated carbons derived from waste sugarcane bagasse for CO2 adsorption. *Chemical engineering journal*, *381*, 122736. https://doi.org/10.1016/j.cej.2019.122736

He, Y., Zhang, Y., Li, X., Lv, Z., Wang, X., Liu, Z., & Huang, X. (2018). Capacitive mechanism of oxygen functional groups on carbon surface in supercapacitors. *Electrochimica Acta*, *282*, 618–625. https://doi.org/10.1016/j.electacta.2018.06.103

Hidayati, A. S. D. S. N., Kurniawan, S., Restu, N. W., & Ismuyanto, B. (2016). Potential of Sugar Cane As an Alternative Raw Material for Making Activated Carbons. *Natural B, Journal of Health and Environmental Sciences*, *3*(4), 318–322. http://dx.doi.org/10.21776/ub.natural-b.2016.003.04.8

Jagadale, A., Zhou, X., Xiong, R., Dubal, D. P., Xu, J., & Yang, S. (2019). Lithium ion capacitors (LICs): Development of the materials. *Energy Storage Materials*, *19*, 314-329. https://doi.org/10.1016/j.ensm.2019.02.031

Jain, A., & Tripathi, S. K. (2015). Nano-porous activated carbon from sugarcane waste for supercapacitor application. *Journal of Energy Storage*, *4*, 121–127. https://doi.org/10.1016/j.est.2015.09.010

Ju, J., Zhang, L., Shi, H., Li, Z., Kang, W., & Cheng, B. (2019). Three-dimensional porous carbon nanofiber loading MoS2 nanoflake-flowerballs as a high-performance anode material for Li-ion capacitor. *Applied Surface Science*, *484*, 392–402. https://doi.org/10.1016/j.apsusc.2019.04.099

Kumar, A., Khandelwal, M., Gupta, S. K., Kumar, V., & Rani, R. (2019). Fourier transform infrared spectroscopy: Data interpretation and applications in structure elucidation and analysis of small molecules and nanostructures. In *Data Processing Handbook for Complex Biological Data Sources* (pp. 77-96). Academic Press. https://doi.org/10.1016/B978-0-12-816548-5.00006-X

Li, B., Dai, F., Xiao, Q., Yang, L., Shen, J., Zhang, C., & Cai, M. (2016). Activated carbon from biomass transfer for high-energy density lithium-ion supercapacitors. *Advanced Energy Materials*, *6*(18), 1600802. https://doi.org/10.1002/aenm.201600802

Lin, Y. T., Chang-Jian, C. W., Hsieh, T. H., Huang, J. H., Weng, H. C., Hsiao, Y. S., ... & Chen, C. P. (2021). High-performance Li-Ion capacitor constructed from biomass-derived porous carbon and high-rate Li4Ti5O12. *Applied Surface Science*, *543*, 148717. https://doi.org/10.1016/j.apsusc.2020.148717

Liu, S., Sun, J., & Huang, Z. (2010). Carbon spheres / activated carbon composite materials with high Cr (VI) adsorption capacity prepared by a hydrothermal method. *Journal of Hazardous Materials*, *173*, 377–383. https://doi.org/10.1016/j.jhazmat.2009.08.086

Liu, X.-Y., Huang, M., Ma, H.-L., Zhang, Z.-Q., Gao, J.-M., Zhu, Y.-L., Han, X.-J., & Guo, X.-Y. (2010). Preparation of a carbon-based solid acid catalyst by sulfonating activated carbon in a chemical reduction process. *Molecules*, *15*(10), 7188–7196. https://doi.org/10.3390/molecules15107188

Lu, P., Huang, Q., Chi, Y., & Yan, J. (2017). Preparation of high catalytic activity biochar from biomass waste for tar conversion. *Journal of Analytical and Applied Pyrolysis*, *127*, 47–56. https://doi.org/10.1016/j.jaap.2017.09.003

Luo, X., Cai, Y., Liu, L., & Zeng, J. (2019). Cr(VI) adsorption performance and mechanism of an effective activated carbon prepared from bagasse with a one-step pyrolysis and ZnCl2 activation method. *Cellulose*, *26*. https://doi.org/10.1007/s10570-019-02418-9

Nitta, N., Wu, F., Lee, J. T., & Yushin, G. (2015). Li-ion battery materials: present and future. *Materials Today*, *18*(5), 252–264. https://doi.org/10.1016/j.mattod.2014.10.040

Nowrouzi, M., Behin, J., Younesi, H., Bahramifar, N., Charpentier, P. A., & Rohani, S. (2017). An enhanced counter-current approach towards activated carbon from waste tissue with zero liquid discharge. *Chemical Engineering Journal*, *326*, 934–944. https://doi.org/10.1016/j.cej.2017.05.141

Okamura, M., Takagaki, A., Toda, M., Kondo, J. N., Domen, K., Tatsumi, T., Hara, M., & Hayashi, S. (2006). Acid-catalyzed reactions on flexible polycyclic aromatic carbon in amorphous carbon. Chemistry of Materials, 18(13), 3039–3045.

Oliveira, F. M. V, Pinheiro, I. O., Souto-Maior, A. M., Martin, C., Gonçalves, A. R., & Rocha, G. J. M. (2013). Industrial-scale steam explosion pretreatment of sugarcane straw for enzymatic hydrolysis of cellulose for production of second generation ethanol and value-added products. *Bioresource Technology*, *130*, 168–173.
https://doi.org/10.1016/j.biortech.2012.12.030

Pandey, A., Soccol, C. R., Nigam, P., & Soccol, V. T. (2000). Biotechnological potential of agro-industrial residues. I: sugarcane bagasse. *Bioresource Technology*, *74*(1), 69–80
https://doi.org/10.1016/S0960-8524(99)00142-X.

Pramono, A. E., Nura, M. Z., Soedarsono, J. W. M., & Indayaningsih, N. (2019). Effect of sintering temperature on the relationship of electrical conductivity and porosity characteristics of carbon ceramic composites. Journal of Ceramic Processing Research, 20(4), 333–346.

Rahma, N. A., Kurniasari, A., Pambudi, Y. D. S., Bintang, H. M., Zulfia, A., & Hudaya, C. (2019). Characteristics of Corncob-Originated Activated Carbon Using Two Different Chemical Agent. In IOP Conference Series: Materials Science and Engineering (Vol. 622, No. 1, p. 012030). IOP Publishing.

Rajarao, R., Mansuri, I., Dhunna, R., Khanna, R., & Sahajwalla, V. (2014). Characterization of gas evolution and char structural change during pyrolysis of waste CDs. *Journal of Analytical and Applied Pyrolysis*, *105*, 14–22.
https://doi.org/10.1016/j.jaap.2013.09.014

Salman, J. M. (2014). Optimization of preparation conditions for activated carbon from palm oil fronds using response surface methodology on removal of pesticides from aqueous solution. *Arabian Journal of Chemistry*, *7*(1), 101–108.
https://doi.org/10.1016/j.arabjc.2013.05.033

Savéant, J. M. (2006). Elements of molecular and biomolecular electrochemistry: an electrochemical approach to electron transfer chemistry. John Wiley & Sons.

Simon, P., & Gogotsi, Y. (2010). Materials for electrochemical capacitors. In *Nanoscience and technology: A Collection of Reviews from Nature Journals. World Scientific.* (pp. 320–329).
https://doi.org/10.1142/9789814287005_0033

Sun, F., Liu, X., Wu, H. B., Wang, L., Gao, J., Li, H., & Lu, Y. (2018). In situ high-level nitrogen doping into carbon nanospheres and boosting of capacitive charge storage in both anode and cathode for a high-energy 4.5 V full-carbon lithium-ion capacitor. Nano letters, 18(6), 3368-3376.

Tajalli, A. (2015). Panduan penilaian potensi biomassa sebagai sumber energi alternatif di indonesia. Penabulu Alliance.

Timur, S., İkizoğlu, E., & Yanik, J. (2006). Preparation of Activated Carbons from Oreganum Stalks by Chemical Activation. *Energy & Fuels - ENERG FUEL*, *20*.
https://doi.org/10.1021/ef060219k

Wibowo, S., Syafi, W., & Pari, G. P. (2011). Karakterisasi permukaan arang aktif tempurung biji nyamplung. Makara Journal of Technology, 15(1), 150718.

Xie, J., Yang, P., Wang, Y., Qi, T., Lei, Y., & Li, C. M. (2018). Puzzles and confusions in supercapacitor and battery: theory and solutions. *Journal of Power Sources*, *401*, 213–223.
https://doi.org/10.1016/j.jpowsour.2018.08.090

Yang, H., Yan, R., Chen, H., Lee, D. H., & Zheng, C. (2007). Characteristics of hemicellulose, cellulose and lignin pyrolysis. *Fuel*, *86*(12–13), 1781–1788.
https://doi.org/10.1016/j.fuel.2006.12.013

Zeng, L., Qiu, L., & Cheng, H.-M. (2019). Towards the practical use of flexible lithium ion batteries. *Energy Storage Materials*, *23*, 434–438.
https://doi.org/10.1016/j.ensm.2019.04.019

Zhang, F., Zhang, T., Yang, X., Zhang, L., Leng, K., Huang, Y., & Chen, Y. (2013). A high-performance supercapacitor-battery hybrid energy storage device based on graphene-enhanced electrode materials with ultrahigh energy density. *Energy and Environmental Science*, *6*(6), 1623–1632.
https://doi.org/10.1039/c3ee40509e

Zurutuza, A., & Marinelli, C. (2014). Challenges and opportunities in graphene commercialization. *Nature Nanotechnology*, *9*(10), 730–734.
https://doi.org/10.1038/nnano.2014.225